Proton transfer in [HEIM][TFSI] ionic liquid: insights from polarisable and neural network simulations

Martín Otero-Lema,[1,2] Kateryna Goloviznina,[3,4] Luis Miguel Varela,[1,2] Mathieu Salanne,[3,4,5] Hadrian Montes-Campos,[1,2,a)] and Alessandra Serva[3,4,b)]

[1)] *Grupo de Nanomateriais, Fotónica e Materia Branda, Departamento de Física de Partículas, Universidade de Santiago de Compostela, Campus Vida s/n, E-15782, Santiago de Compostela, Spain*

[2)] *Instituto de Materiais (iMATUS), University of Santiago de Compostela, Campus Vida s/n, Santiago de Compostela, 15782, Spain*

[3)] *Sorbonne Université, CNRS, Physicochimie des Électrolytes et Nanosystèmes Interfaciaux, F-75005 Paris, France*

[4)] *Réseau sur le Stockage Electrochimique de l'Energie (RS2E), FR CNRS 3459, 80039 Amiens Cedex, France*

[5)] *Institut Universitaire de France (IUF), 75231 Paris, France*

(Dated: 10 January 2025)

Protic ionic liquids, PILs, are promising materials for energy storage applications, in part due to their ability to decouple proton transport from ion diffusion. In this work, the proton transfer mechanism in 1-ethylimidazolium bis(trifluoromethanesulfonyl)imide ([HEIM][TFSI]) IL was studied by means of three different computational approaches. Classical polarizable molecular dynamics simulations were used to explore the structure and dynamics of the fully ionized system, while Density Functional Theory calculations were carried out to estimate the energy barriers for the different proton transfer reactions. Finally, the proton transfer was explicitly studied by means of Neural Network Force Field simulations. Our results show that this reaction is indeed possible when doping the IL with an excess of deprotonated cations, and highlight the importance of the formation of dimers between donor and acceptor species for the proton transfer to occur. The main driving factor for the reaction was found to be the energy cost for reaching a suitable coordination environment and form such dimers, which is higher than that for the transfer reaction.

I. INTRODUCTION

The ability to store energy is essential for meeting the ever-increasing demands of modern society. To transition from fossil fuels to sustainable energy sources, electrochemical energy storage becomes particularly crucial in ensuring a steady power supply while relying on renewable energy sources such as wind or solar, which are intermittent by nature. Nowadays, the use of electrochemical devices such as lithium-ion batteries[1] (LIBs) and supercapacitors[2] (SCs) is widespread. However, these devices can be hazardous due to the volatility and flammability of the electrolytes needed for their operation.[3,4] Significant efforts have been made to research alternative electrolytes that do not suffer from these problems, while retaining or improving the energy storage capabilities of classical electrolytes.

Ionic Liquids (ILs) have emerged as one of the leading candidates for next-generation electrolytes.[5–7] ILs are composed entirely of cations and anions and can remain liquid at room temperature due to the difference in size between the ions. This asymmetry hinders tight packing, and thus allows thermal vibrations to overcome the Coulomb forces holding them together. ILs exhibit very desirable properties as electrolytes, such as negligible vapor pressure due to the high electrostatic forces between their components, and high thermal stability. These properties make them interesting candidates for novel low-risk LIBs or SCs.[8–12] Moreover, the wide array of available cations and anions allows for a high degree of customizability, enabling to fine-tune the properties of the electrolyte. Nevertheless, ILs suffer from high viscosities and low diffusivities, which can hinder their applicability in electrochemical devices, where fast charge transport in the electrolyte is desired.[13]

In recent years, much effort has been devoted to the experimental characterization of PIL-based electrochemical devices.[14,15] Special attention has been paid to studying the interplay between the electrode and the electrolyte, and the phenomenon of pseudocapacitance. Materials such as RuO_2, VN and TiN have been found to favour proton transfer between the PIL and the surface.[16–18] Activated carbons have also received attention, since the porous cavities present in these materials can enhance both electrolyte wetting and capacitance,[19] while the introduction of functional groups into the carbon matrix was found to increase pseudocapacitance.[20]

Theoretical methods have been used to probe the nanostructure of PILs and to complement experimental findings, providing resolution at molecular level. In previous works, the properties of mixtures of PILs with different solvents were studied and compared to those of aprotic ILs, both in bulk and at interfaces.[21–23] The effect of water on these electrolytes has also been extensively studied, since large aggregation of water near

[a)] Electronic mail: hadrian.montes@usc.es
[b)] Electronic mail: alessandra.serva@sorbonne-universite.fr

the electrode can cause stability issues.[24,25] Recently, A. Balducci *et al.* have investigated the properties of a novel water-in-PIL electrolyte both experimentally and by means of classical Molecular Dynamics (MD), showing that despite the hygroscopic nature of PILs, it is possible to avoid unwanted reactions at the electrode.[26,27]

When it comes to the simulation of PILs, recent developments in simulation techniques have made it possible to correctly describe the phenomena that govern them. On the one hand, the development of polarizable force fields allows for a correct accounting of the dynamics, and for a more robust description of the hydrogen bond network that permeates them.[28–30] On the other hand, proton transfer reactions that take place within some PILs have historically necessitated *ab initio* methods to be reproduced,[31] which are usually very limited in size and time scales that can be investigated. Recently, the rise in popularity of neural networks has lead to the development of neural network force fields (NNFFs) that can extend these scales while retaining the characteristic accuracy of *ab initio* calculations.[32] Nevertheless, the size of NNFF simulations is still limited to a few hundred molecules compared to polarizable MD simulations, the latter remaining the clear favourite for the simulation of large periods of time and large systems. Recently, Joerg *et al.* introduced `protex`, a tool for the simulation of proton transfer in ILs that, while still relying on a force field parametrization, is able to capture proton dynamics using a polarizable force field with a reduced computational cost.[33,34]

In this work, we study the proton transfer mechanism in 1-ethylimidazolium bis(trifluoromethanesulfonyl)imide ([HEIM][TFSI]) IL at different length and time scales. The system is similar to the one previously studied by Hoarfrost and coworkers, who found evidence of proton transfer in mixtures of this PIL with imidazole by means of Nuclear Magnetic Resonance[35] (NMR). This was later confirmed by Mosses *et al.* using *ab initio* MD.[36] However, the proton transfer process in the neat IL, as well as its mixtures with protonated or deprotonated variants of the anion and cation, respectively, has received little attention so far. It is thus the focus of this work. First, a polarizable force field was developed to describe the different chemical species. It was used to analyze the structure and dynamics of the PIL, as well as to shed light on the possible proton transfers in the system. Then, the energy barriers of the proton transfer reaction were characterized by means of quantum mechanical calculations at the Density Functional Theory (DFT) level. Finally, MD simulations using a NNFF were carried out to examine the proton hopping within the IL medium.

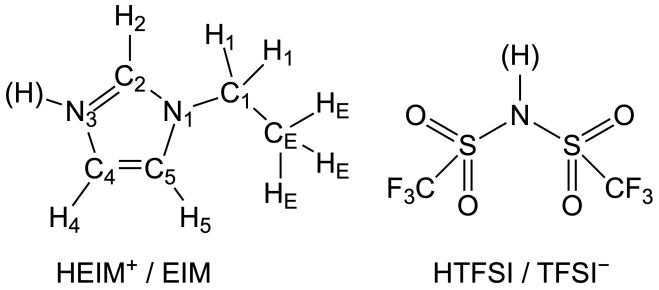

FIG. 1. Structural formulae of cation, anion, and neutral species with corresponding labels. Please note that we refer to $[HEIM]^+$ also as HC^+, [EIM] as C, [HTFSI] as HA and $[TFSI]^-$ as A^-, respectively.

II. METHODS

A. Polarizable classical MD simulations

Atomistic MD simulations were carried out in OpenMM[37] software, version 7.6. Two systems containing a total of 600 molecules/ion pairs were considered: a purely ionic, with a 1:1 ratio of $[HEIM]^+$ cations and $[TFSI]^-$ anions, and a 50% ionic, formed by a 1:1:1:1 ratio of cations, anions and neutral [EIM] and [HTFSI] species. The corresponding structural formulae are given in Fig. 1.

A polarizable force field was first developed for $[HEIM]^+$, [EIM] and [HTFSI] using the CL&Pol approach.[38] For the charged species, non polarizable parametrization was taken from the CL&P force field[39] and used as a starting point to build the polarizable models, whereas for the neutral molecules a non polarizable model had to be built before introducing polarization effects (see Supporting Information for all the details).

The simulation procedure was the same for all systems. Initial configurations were built using PACKMOL[40] and `fftool`,[41] and force field files for OpenMM were created with `pol_openmm`.[42] The systems underwent a 10 ns equilibration in the NpT ensemble, followed by another 5 ns equilibration in the NVT ensemble. Finally, 50 ns production runs in the NVT ensemble were carried out using a timestep of 1 fs. Three independent replicas were simulated for each system, starting from different configurations, in order to adequately sample the phase space. The reported properties were calculated as averages over these replicas. During production runs, positions of all particles were recorded every 0.5 ps, while the electric current vector was recorded at every timestep. For all simulations, temperature was kept at a constant value of 298.15 K by means of a temperature grouped Nose-Hoover thermostat,[43,44] whereas in the NpT simulations, pressure was held at 1 atm by means of a Monte Carlo barostat.[45,46] More details on the simulation setup can be found in the Supporting Information.

B. DFT calculations

Density functional theory calculations at B3LYP/6-311++G(d,p) level were used to quantify the probability of the proton transfer reactions. Representative molecular pairs were extracted from the classical MD simulations, and the energy profile was calculated. This was done by gradually increasing the donor-proton distance while allowing the rest of the structure to relax at each step.[47] The effect of the medium was taken into account through a mean field approach (see Supporting Information for more details).

Once the energy profile along the reaction coordinate was calculated, in order to estimate the reaction probability we followed the approach that Jacobi and coworkers previously used for the 1-methylimidazolium acetate IL.[47] The normalized Maxwell-Boltzmann kinetic energy distribution for the protonated molecule is given by

$$f(E_k) = \beta^2 E_k e^{-\beta E_k} \tag{1}$$

where E_k is the kinetic energy, and $\beta = (k_B T)^{-1}$, with T absolute temperature and k_B Boltzmann's constant. The reaction probability was then given by the probability that a molecule reaches a kinetic energy higher than the energy barrier

$$p = \int_{\Delta E}^{\infty} f(E_k) dE_k \tag{2}$$

where ΔE is the height of the energy barrier in the direction of the reaction. The above equation can be integrated directly to yield the following probability

$$p = (1 + \beta \Delta E)\, e^{-\beta \Delta E} \tag{3}$$

C. Neural network force field simulations

The NNFF simulations were carried out using the most recent version of the NeuralIL force field.[48] The NNFF was developed using configurations extracted from polarizable MD simulations with a reduced set of molecules (7 ion pairs and 5 neutral molecules). DFT calculations using GPAW[49] with the vdW-DF exchange and correlation functional[50] and double zeta polarized basis set were carried out to obtain the energies and forces of 500 configurations extracted from polarizable MD. These data were used to train a first-generation NN which was used to perform short simulations (250 fs). From these new simulations other 500 configurations were extracted and their energy and forces calculated using DFT. Finally, with a total of 1000 configurations a second generation NN was trained, which was the one used for the production simulations. Note that this process does not introduce any bias towards proton transfers. However, it was found that proton transfer was explored by the NN in the second training batch, as it can be seen in Fig. S4 of the SI.

The production simulations were performed on larger systems using JAX MD[51] in the NVT ensemble for 500 ps at 448K using a Nosé-Hoover thermostat.[52] The initial configurations were generated using polarizable MD in the NpT ensemble, and consisted of 90 ion pairs and 10 neutral molecules (either EIM or HTFSI). To analyze proton transfer during the simulations, cage correlation functions (CACFs) between hydrogen and donor atoms were computed. These functions are given by

$$c_{ij}(t) = \frac{\langle \theta_{ij}(t) \cdot \theta_{ij}(0) \rangle}{\langle \theta_{ij}^2 \rangle}, \tag{4}$$

where θ_{ij} takes a value of 1 if the distance between the two particles is less than a given cutoff r_0 and 0 otherwise. The cutoff distances were selected based on coordination distances, since they can be interpreted as the equilibrium distances for a given bond.

III. RESULTS AND DISCUSSION

A. Polarizable classical MD simulations

We considered two systems, the first one purely ionic, consisting of a 1:1 ratio of $[HEIM]^+$ cations and $[TFSI]^-$ anions, the second one a 50% ionic system, formed by a 1:1:1:1 ratio of cations, anions and neutral [EIM] and [HTFSI] species. It should be noted that experimentally the high acidity of the proton in [HTFSI] causes it to fully ionize by transferring its proton to [EIM].[53] Because of this, the pure ionic system is the one that better represents the experimental conditions, while the 50% ionic one is used solely to gain access to the coordination between both charged and neutral species. Therefore, the calculated properties of the 50% ionic system should not be compared with experiments, even though some of the structural features discussed below could be achieved experimentally by adding an excess of either [EIM] or [HTFSI] to the pure IL.

1. Force field validation

Since the main advantage of polarizable force fields over their non-polarizable counterparts is the accurate prediction of dynamic properties,[54] we validate our model for pure [HEIM] [TFSI] by computing viscosity, electric conductivity and ion diffusion coefficients. Details on the calculations can be found in the Supporting Information. The results are reported in Table I, together with the calculated density.

In the case of density, a very good agreement is obtained between simulation and experiment, with a relative error of −0.28 %. For dynamic properties, the

	Simulation	Exp
ρ / g cm^{-3}	1.5685(25)	1.5729[55]
η / Pa s	0.0583(16)	0.0388[56]
σ / S m^{-1}	0.270(18)†	0.368(15)[55]
	0.279(43)‡	0.425(43)[57]
	0.549(22)§	0.244(11)[58]
D_{cat} / 10^{-11} m^2 s^{-1}	1.84(10)	2.51(83)[58]
D_{an} / 10^{-11} m^2 s^{-1}	1.68(10)	-

TABLE I. Calculated density (ρ), viscosity (η), electric conductivity (σ) and diffusion coefficients (D) of pure [HEIM][TFSI], compared to experimental values from the literature. The values are averaged between the three replicas, while the uncertainty is estimated from the standard deviation between replicas. Diffusion coefficients and Nernst-Einstein conductivities include the Yeh-Hummer correction.[59,60] Conductivities are calculated using the Green-Kubo[61] (†), the Einstein-Helfhand[62,63] (‡) and the Nernst-Einstein[64] (§) methods, respectively.

agreement is lower, but in all cases the same order of magnitude is obtained. In general, the predicted dynamics seem to be slightly slower than the experimental one, as evidenced by the higher computational viscosity and the lower diffusion coefficients and electric conductivity. Regarding the latter, three different methods have been used to compute it: the Einstein-Helfhand (EH), the Green-Kubo (GK) and the approximate Nernst-Einstein (NE) methods (see Supporting Information for the details). The comparison between the EH and GK calculations with the approximate NE relation reveals that anion-cation correlations within the liquid contribute significantly to the electric conductivity, lowering its value by approximately a factor of two when compared with the ideal (NE) case. Finally, it is interesting to remark that the obtained GK and EH values are in good agreement with each other, up to statistical uncertainty. When neutral [EIM] and [HTFSI] are added, both viscosity and density decrease, while diffusion coefficients and conductivity increase (see Supporting Information). This is expected as charged species are substituted with their neutral counterparts, and the system becomes less bound via Coulomb interactions, which should lead to faster dynamics. In conclusion, the predicted dynamic properties are in good agreement with the experiments, and the changes induced by the addition of neutral molecules are in line with expectations. Therefore, the developed force field was deemed to be suitable for modelling the behaviour of these mixtures.

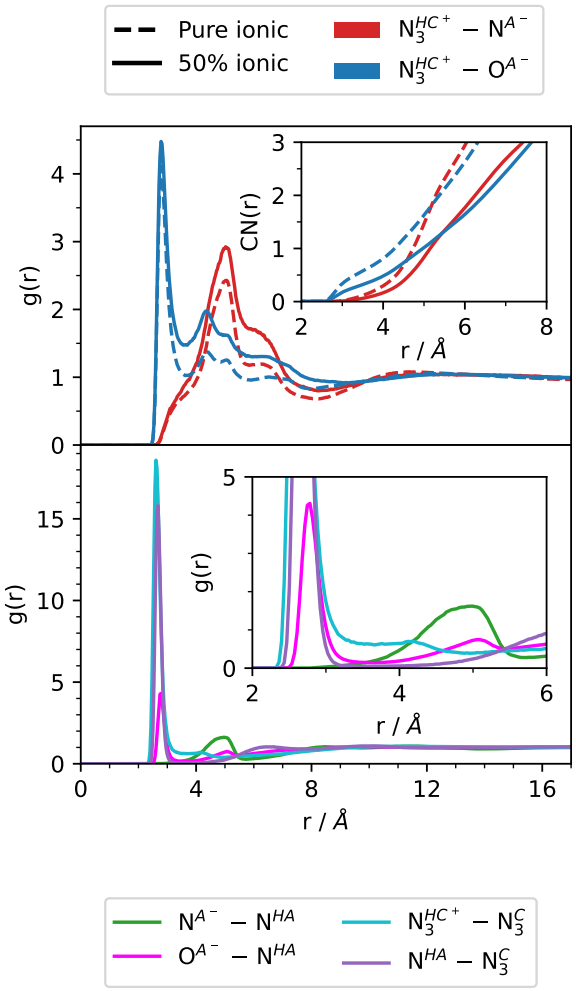

FIG. 2. RDFs between characteristic atoms of each molecule. The atom labels are given in Fig. 1, and we refer to $[HEIM]^+$ as HC^+, [EIM] as C, [HTFSI] as HA and $[TFSI]^-$ as A^-, respectively. The inset in the top panel displays the coordination numbers of anion atoms around the reference atom.

2. *Structural organization of the liquid*

In order to study the structure of the system, we calculated radial distribution functions (RDFs), between representative atoms of each species for both the pure ionic and 50% ionic systems.

The RDFs corresponding to the cation-anion interaction are shown in Fig. 2 (top) and in Fig. S8 of the Supporting Information. The coordination structure remains mostly unchanged when neutral species are added to the system since no changes in the main coordination distances are observed. In particular, the donor nitrogen atom of $[HEIM]^+$ has a greater affinity for the oxygen atoms of $[TFSI]^-$ than for the nitrogen atom. Moreover, as it can be seen in the inset of Fig. 2(top), the coordi-

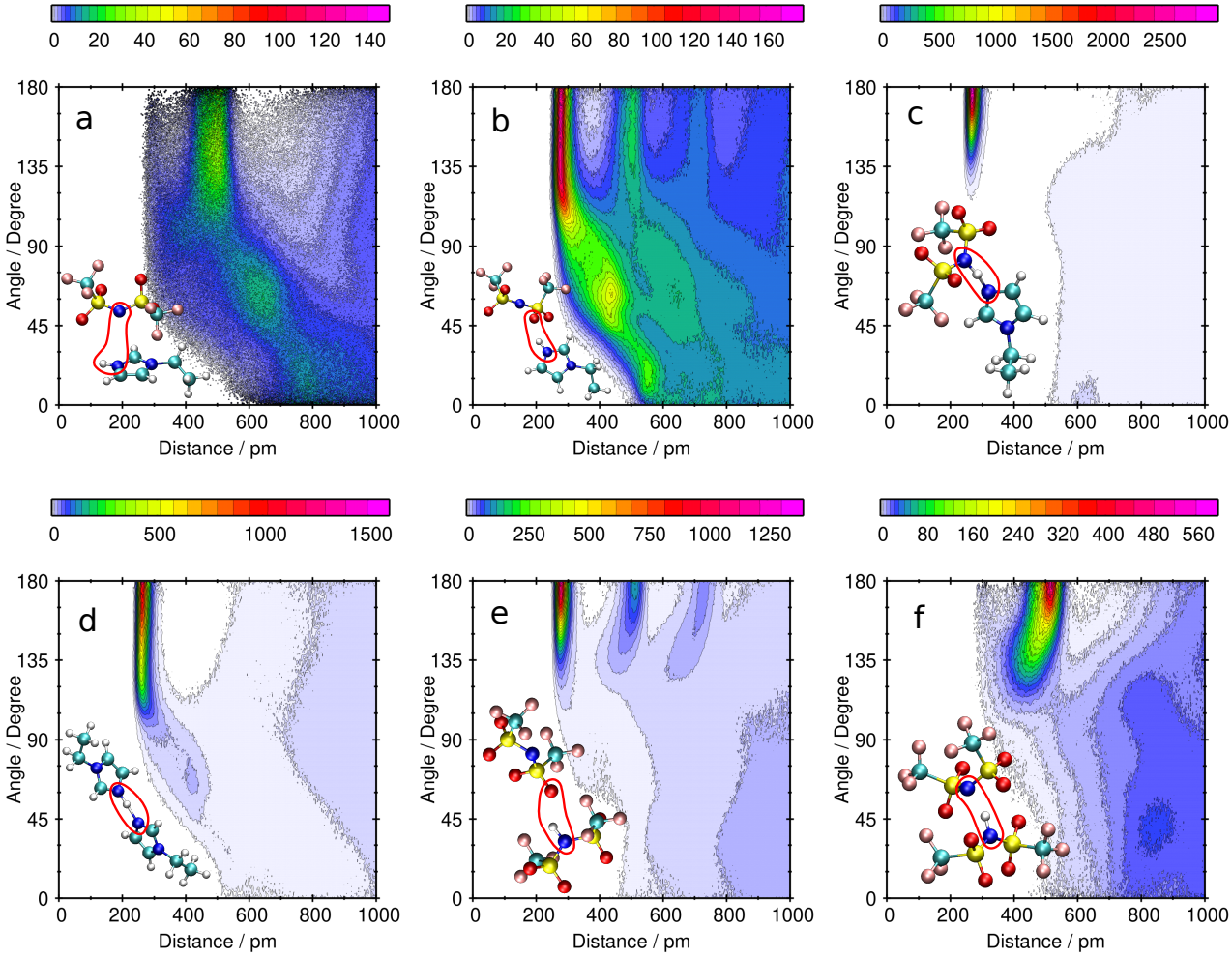

FIG. 3. Combined distribution functions between the donor-acceptor distance (x-axis) and the donor-hydrogen-acceptor angle (y-axis) for different molecules and sites, as well as representative molecular pairs taken from the MD simulation. The colormap reflects the occurrence probability. The donor-acceptor pairs are: a) N_3^+ atom in $[HEIM]^+$ and N^- in $[TFSI]^-$, b) N_3^+ atom in $[HEIM]^+$ and O^- atoms in $[TFSI]^-$, c) N^0 in [HTFSI] and N_3^0 atom in [EIM], d) N_3^+ atom in $[HEIM]^+$ and N_3^0 atom in [EIM], e) N^0 in [HTFSI] and O^- in $[TFSI]^-$, f) N^0 in [HTFSI] and N^- in $[TFSI]^-$. The selected atoms are circled in red for ease of viewing.

nation between the cation and the O atoms in $[TFSI]^-$ is one-to-one (i.e the $[TFSI]^-$ coordinates the cation in a monodentate way), since at the coordination distance the CN is less than one in both cases.

In Fig. 2 (bottom), the RDFs involving atoms of the neutral molecules are displayed. Concerning [EIM] molecules, their nitrogen atoms, $N_3{}^C$, have strong affinities for the donor nitrogen atoms of both $[HEIM]^+$ cations and [HTFSI] molecules, hinting at the possible formation of hydrogen bonds between these species. Regarding the coordination between [HTFSI] and $[TFSI]^-$, the nitrogen atom in the neutral species, N^{HA}, shows very different coordinations with the oxygen and nitrogen atoms of the anion. In the case of oxygen atoms, a short range of coordination distances are found, while in the case of the nitrogen atom, a wider range is observed. This suggests that the most probable coordination is with O atoms, and that the broad distribution in the $N_3^{HC^+}$ - N_3^C RDF corresponds to said coordinations viewed from the reference N atom, as will be further discussed later.

To further investigate the different coordination environments of hydrogen atoms, combined distribution functions (CDFs) between the donor - acceptor atoms distance (x-axis) and the donor-hydrogen-acceptor angle (y-axis) were calculated from the simulation of the 50% ionic system. The results are shown in Fig. 3, along with representative MD snapshots of each molecular pair considered. For the cation-anion interaction (Figs. 3a and 3b), the donor atom of $[HEIM]^+$ forms a hydrogen bond with an oxygen atom of $[TFSI]^-$, as also shown in the snap-

shot. However, that hydrogen bond is not formed with the nitrogen atom of the anion, which is the reason for the larger coordination distances observed in the RDF of Fig. 2. These two coordination modes can be analyzed in conjunction with previous experimental findings. Hoarfrost and coworkers[35] found through NMR spectroscopy that no proton conduction occurs in the pure IL. This is consistent with our simulations which do not show a N-H-N hydrogen bond between cations and anions, which could lead to the formation of a pair of neutral molecules and thus contribute to proton conduction. Furthermore, it must be the case that the N-H-O hydrogen bond found in the simulations does not lead to proton transfer, since that would also induce proton conduction.

The structure of [HTFSI] and [EIM] (Fig. 3c) is also revealing of the experimental properties of the pure liquid. A hydrogen bond is formed between the two species, in contrast with Fig. 3a, where the proton is bound to the cation. This hydrogen bond allows for the ionization of a pair of neutral molecules into a cation-anion pair, as will be discussed later. This is again consistent with experimental findings, which indicate that stequiometric amounts of [EIM] and [HTFSI] ionize each other.[53]

Regarding the $[HEIM]^+$-[EIM] pair, Fig. 3d shows that they form a hydrogen bond, which should enable proton conduction, as observed experimentally when an excess of deprotonated cations are added to the pure IL.[35] Finally, two different coordination modes can be found between [HTFSI] and $[TFSI]^-$. The first one, in Fig. 3e, shows a shorter coordination distance, as found in the RDF of Fig. 2, and it corresponds to the formation of a hydrogen bond between an oxygen atom in the anion and the nitrogen atom in the neutral molecule. On the other hand, the coordination displayed in Fig. 3f is more interesting, and reveals a proton bridge structure between the two moieties, in a wide range of distances between donor and acceptor. Both these coordinations were found in a study by Munson and coworkers using NMR spectroscopy in conjunction with *ab initio* calculations.[65] Of the two structures, the proton bridge stands out, as it could enable proton transfer between the two species when an excess of [HTFSI] is added to the pure IL. However, the proton bridge structure is the least common of the two, since the high probability region in Fig. 3f corresponds to the N-N distance for the other dimer. The N-N coordination distance for the proton bridge structure was found to be around 2.7 Å by inspecting the MD snapshots. From the RDF of Fig. 2b, it can be seen that, even though the probability of such a coordination is not zero, it is very low compared to the N-H-O hydrogen bond.

B. DFT proton transfer barriers

As discussed earlier, the existence of hydrogen bonds between different moieties in the system hints at the possibility of proton transfer between those species. The corresponding calculated energy profiles, as well as the probabilities for the forward and backward reactions, are shown in Fig. 4. Panel 4a refers to the proton transfer from $[HEIM]^+$ to [EIM]. Symmetrical energy profiles are found for the forward and backward reactions, since the reactants and the products are the same. The reaction probabilities have values around 20%, showing that the proton transfer mechanism between these molecules is indeed possible. In Fig. 4b the energy profile for the proton transfer between $[TFSI]^-$ and [HTFSI] in the bridged structure (see snapshot of Fig. 3f) is reported. The proton transfer is possible, albeit with lower probabilities than for $[HEIM]^+$/[EIM]. This, together with the scarcity of the proton bridge structure, could explain why the contribution of hopping to proton conduction is greater when adding [EIM] than when adding [HTFSI].[35] Interestingly, the barrier heights are not symmetric for

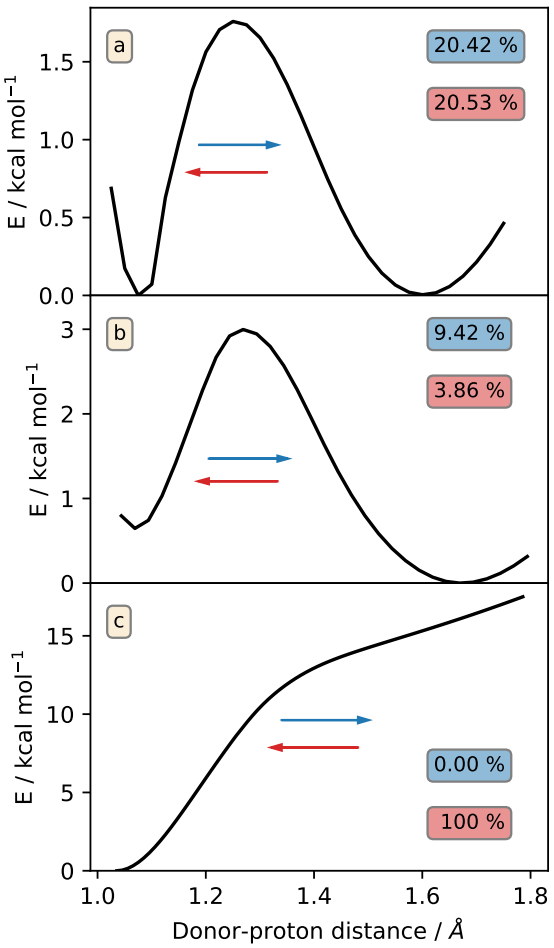

FIG. 4. Energy profiles for the different proton transfer reactions, as well as the calculated jumping probabilities. a: $[HEIM]^+ + [EIM] \rightleftharpoons [EIM] + [HEIM]^+$, b: $[HTFSI] + [TFSI]^- \rightleftharpoons [TFSI]^- + [HTFSI]$, c: $[HEIM]^+ + [TFSI]^- \rightleftharpoons [EIM] + [HTFSI]$.

the reactions, reflected by the unequal forward and backward reaction probabilities. This is due to the fact that the reaction involves two conformational isomers, as seen in the snapshot of Fig. 3f, i.e the proton transfer takes place between a cis-trans pair of anions. Therefore, the energy difference between the two minima can be understood in terms of the different bonding energies of the proton to each of the isomers.

Finally, in Fig. 4c the energy barrier for the transference of a proton from $[HEIM]^+$ to $[TFSI]^-$ is represented. Only one minimum is found, corresponding to the ionized state, meaning that the product state is not stable. This is consistent both with the coordination between the two ions, which does not involve a hydrogen bond, and with the coordination between neutral [EIM] and [HTFSI], which does. Indeed, the calculated energy profile suggests that as soon as a hydrogen bond is formed between the neutral molecules, a proton transfer reaction happens and leads to the formation of a cation-anion pair, which is no longer hydrogen bonded, and thus the backward reaction is not possible. Thus, mixing neutral molecules in equal amounts will result in a pure IL where no proton transfers take place, as previously mentioned.

C. Neural network force field simulations

NNFF simulations were performed for two systems, containing an excess of EIM or HTFSI, respectively. To study the proton transfer mechanism, we started by investigating the structure between moieties in these new simulations. In Fig. 5 (top) the RDF between mobile hydrogen atoms and donor/acceptor nitrogen atoms is represented. A sharp peak at a distance around 1 Å, which corresponds the hydrogen being covalently bound to the reference atom, can be seen for both systems. Moreover, a secondary coordination distance around 1.5 Å is observed when adding extra [EIM], which, as will be shown later, corresponds to the proton having jumped from the neutral molecule to the cation. For an excess of [HTFSI], a much broader distribution of distances can be observed, ranging from 2 to 5 Å.

To further analyze this difference, RDFs between donor and acceptor sites are displayed in Fig. 5 (bottom). Here a stark contrast between the two systems is observed. In the case of the addition of [EIM], a clear coordination distance of 3 Å can be observed, which agrees with the results of the polarizable simulations (Figs. 2 (bottom) and 3d). It corresponds to a N-H-N hydrogen bond between a $[HEIM]^+$ cation and a [EIM] molecule. On the contrary, when adding an excess of [HTFSI], the coordination distances between anions and [HTFSI] are much broader and take larger values, with no traces of short coordination distances, again following the same tendencies seen in the classical MD simulations. The fact that the shortest coordination distances start at 3 Å signals that all $[TFSI]^-$-[HTFSI] dimers adopt the configuration shown in Fig. 3e, rather than the bridge structure depicted in Fig. 3f and which exhibits a coordination distance of 2.7 Å. Thus, between these species a O-H-N hydrogen bond is formed, rather than a N-H-N bond leading to the bridge structure, and therefore no proton transfer reaction is expected to take place.

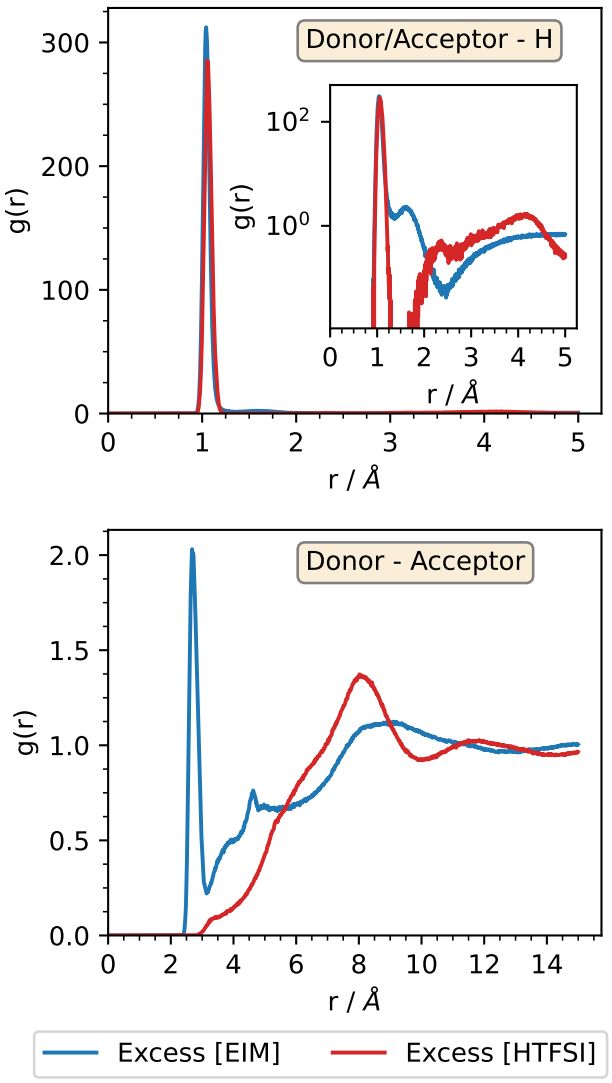

FIG. 5. RDFs between donor/acceptor nitrogen sites ($N_3^{HC^+}$ and N_3^C atoms) and hydrogen atoms (top), and between donor and acceptor sites (bottom) obtained from the NNFF simulations.

In Fig. 6 we represent the CACFs between hydrogen and donor atoms for the system with an excess of [EIM] and for a variety of cutoff distances. These range from 1.3 Å, the coordination distance seen in the RDFs, to slightly larger distances as 1.5 and 2.0 Å. From the correlation functions, it is clear that proton transfer occurs in the system, since the decrease of the CACF for long times indicates that some of the hydrogen atoms left the N atom to which they were originally bonded. Moreover, two different processes can be clearly appreciated. For

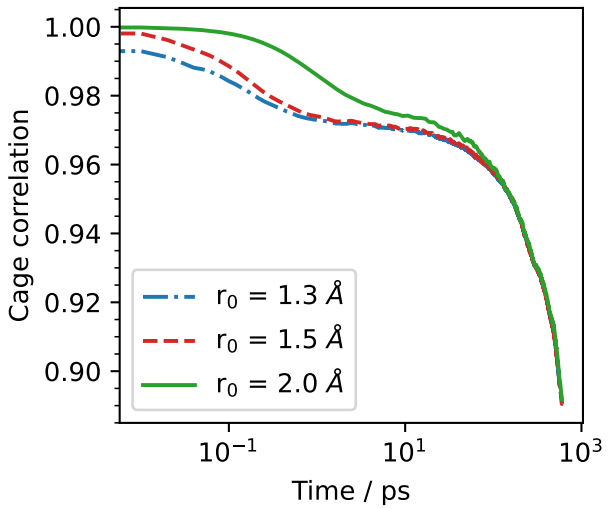

FIG. 6. Cage correlation functions for the hydrogen - donor pairs. Here donors are taken to be both the $N_3^{HC^+}$ and N_3^C atoms, to account for the indistinguishibility of the particles.

short times, the choice of cutoff distance noticeably alters the behaviour of the CACF, whereas for large times, the three curves collapse into one, independently of r_0. The first regime corresponds to the proton hopping back and forth between donor and acceptor, and thus it is sensible to the exact definition of the bound state, while the long time limit can be interpreted as the proton having jumped from the donor to the acceptor, and then for both molecules to have diffused apart. This is to be expected, since once a noticeable number of the molecular pairs have been broken, the specific definition of the bound state will no longer be relevant. As such, the CACFs show evidence for proton diffusion in the [HEIM][TFSI] + [EIM] system. However, when analyzing the trajectories for the [HEIM][TFSI] + [HTFSI] system, no proton jumps were found to take place, consistently with the absence of the proton bridge structure.

To gain some insight as to why no proton diffusion is found in the presence of an excess of [HTFSI], even though the potential energy profiles in Fig. 4 show that it should be possible, energy barriers for the proton transfer reactions were determined from the NNFF simulations. To do so we define a reaction coordinate given by $\xi = r_a - r_d$, where $r_a(r_d)$ is the distance between the acceptor (donor) and the hydrogen atom, projected into the axis that connects the donor and the acceptor (see Fig. S9). Then, the probability that a given donor-acceptor pair has a certain value of this reaction coordinate, $p(\xi)$, is computed from the simulation. Finally, the potential of mean force (PMF), $\Delta E(\xi)$, can be computed as a function of the reaction coordinate as

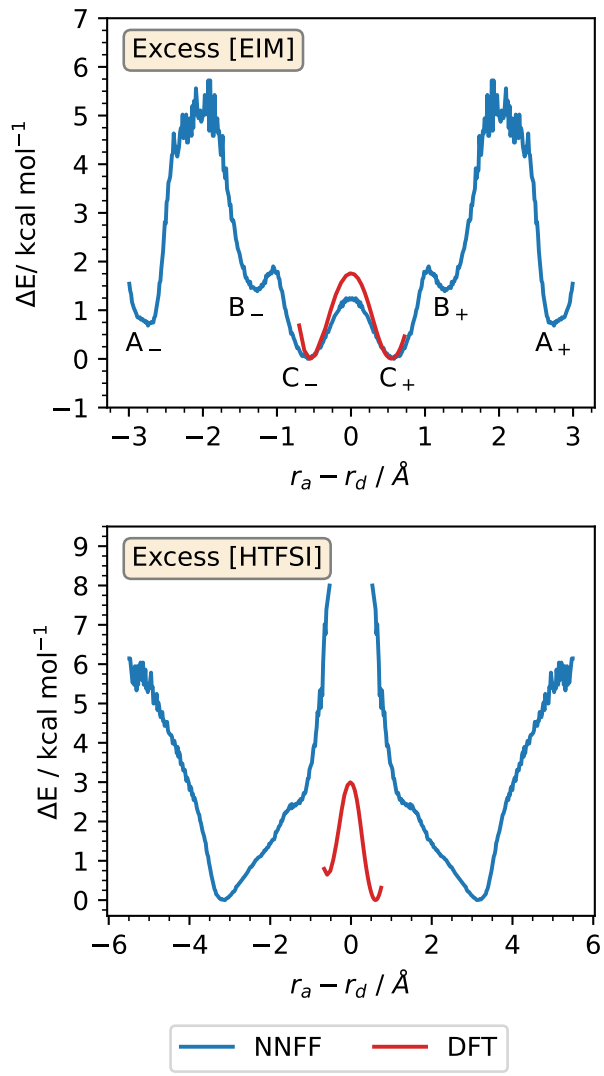

FIG. 7. Potential of mean force and energy profiles obtained from the NNFF simulations and DFT calculations, respectively, for the proton transfer reaction between [EIM] and $[HEIM]^+$ (top) and $[TFSI]^-$ and [HTFSI] (bottom). The energy origins for each curve were chosen as that of their respective minima.

$$\Delta E(\xi) = -k_B T \log p(\xi) \tag{5}$$

Additional details about the calculation of the PMF can be found in the SI. The results are shown in Fig. 7, along with the energy barriers obtained from DFT calculations, expressed in terms of the new reaction coordinate. In the case of excess [EIM], three energy minima, corresponding to stable configurations, can be seen in the PMF. The ones at $\xi = \pm 2.75$ Å (labeled $A_\pm$) correspond to a $[HEIM]^+$ - [EIM] pair that are adjacent to one another but where the coordination is not yet optimal for a proton transfer reaction to take place. This state is

separated by a large energy barrier of ~ 4 kcal/mol (corresponding to $\sim 2.4\ k_BT$ at room temperature) from the most stable configuration, with a value of the reaction coordinate of ± 0.5 (labeled $C_\pm$). This corresponds to a configuration like the one represented in Fig. 3d, where the proton is shared between the two nitrogen atoms, although it is closer to one than to the other. Between these two states, an intermediate configuration is found ($B_\pm$), which could correspond to rearrangements of the N-H-N angle as the two molecules get closer to one another.

The most stable configuration $C_\pm$ has the same values of the reaction coordinate as the energy minima of the energy barriers shown in Fig. 4. This energy was chosen as a common origin for both the PMF and the energy barriers computed through DFT. Both calculations are in excellent agreement with one another, for the location of the minima as well as the width of the proton transfer barrier, although a difference in the height between the NNFF estimate and the one obtained with DFT. This is possibly due to the fact that DFT calculations account for the effect of the environment through a mean field approach, whereas in the NNFF simulations it is done explicitly.

In summary, the mechanism for proton diffusion for the case of excess [EIM] is the following: Once an adjacent donor-acceptor pair overcomes the energy barrier between the $A_\pm$ and $C_\pm$ states, they become coordinated and a process begins where the proton hops between the two molecules, transitioning back and forth between the C_+ and C_- states. At last, if the large barrier is overcome again, it becomes possible for the two molecules to diffuse apart, once the proton has been transferred. A summary of the reaction is shown in Fig. S10 of the SI, as well as a video of the MD simulation.

The case of excess [HTFSI], shown in Fig. 7 (bottom), reveals a similar picture, but with a key difference. Indeed, the PMF displays a single stable state for high reaction coordinates. Moreover, a large energy barrier is found between this stable state and the configurations explored with DFT. This is due to the fact that, as previously mentioned, no proton bridge structures like the one depicted in Fig. 4f are formed in these simulations, and instead a N-H-O hydrogen bond is formed. The energy barrier in the PMF represents the energy cost associated with shift from such a configuration to the N-H-N bridge structure, which seems to be very large. This is in agreement with the polarizable MD simulations, where such structures were rare, and explains why no proton jumps are observed even though the barrier for the proton transfer is relatively small (since even if that is the case, the configuration needed for this reaction is not easily reachable).

Therefore, the NNFF simulations, along with the results presented in the previous section, reveal that the nature of proton transport in the studied systems depends upon two key factors. From one side, the energy barriers of the proton transfer reactions determine whether or not a proton hop can take place once the involved molecules are coordinated and are forming a hydrogen bond. On the other hand, reaching a suitable coordination environment is also important, since the corresponding kinetic barriers were found to be higher than those for the proton transfer reaction.

IV. CONCLUSIONS

In this work, the proton transfer mechanism in 1-ethylimidazolium bis(trifluoromethylsulfonyl)imide IL was studied by means of polarizable MD simulations, quantum mechanical DFT calculations and NNFF MD simulations.

The polarizable CL&Pol force field was extended to describe the pure IL, protonated anions and deprotonated cations. MD simulations of both pure and 50% ionic systems were carried out, revealing the formation of a strong hydrogen bond between [EIM] and [HTFSI]. This reflects the tendency of neutral species to ionize each other to form a cation-anion pair. Moreover, hydrogen bonds between [EIM] and $[HEIM]^+$ were found, as well N-H-N bond between [HTFSI] and $[TFSI]^-$ (even if less probable), which could enable proton transfer when an excess of either neutral species is added to the pure IL.

The analysis of the proton transfer through DFT calculations confirmed that two neutral species undergo irreversible ionization when coming in contact, while the formation of [EIM]-$[HEIM]^+$ or $[TFSI]^-$-[HTFSI] dimers can lead to a proton transfer reaction. Such a transfer is more likely to happen in the excess of [EIM] with energy barriers of 1.5 and 3 kcal/mol, respectively. To study the proton transfer in mixtures of pure IL with an excess of one of the neutral species, a NNFF was developed. Our simulations reveal that proton transfer indeed takes place within the IL + [EIM] mixture, while no jumps were detected when [HTFSI] is added. This discrepancy was resolved through the analysis of the PMFs. For a proton transfer to take place, the involved molecules must overcome an energy barrier to form a dimer. This is possible in the case of the $[HEIM]^+$-[EIM] pair, requiring a barrier of only 4 kcal/mol, but not for [HTFSI]-$[TFSI]^-$, where the barrier reaches 9 kcal/mol.

In conclusion, this study shows that the proton transfer mechanism is driven by two key metrics. On the one hand, the height of the proton transfer barrier between one molecule to another determines if a proton jump is possible once the donor and the acceptor are coordinated and form a dimer. On the other hand, the coordination barrier that the molecules must overcome to form such dimer is also of great importance, since it can prevent otherwise possible proton transfers. These barriers can be accurately captured with NNFF simulations, which achieve the same level of accuracy as DFT results.

Finally, while the developed polarizable force field by its nature cannot take into account proton exchange, it

allows for simulating much larger sizes and time scales than the NNFF. In the future these classical MD simulations could be improved by incorporating proton transfer events, based on DFT reaction probabilities, such as `protex`.[33] This could allow access to rare configurations that are not explored during the NNFF simulations, such as the [HTFSI]-[TFSI]$^-$ proton bridge structure, which will be investigated in upcoming works.

ACKNOWLEDGMENTS

The financial support of the Spanish Ministry of Science and Innovation (PID2021-126148NA-I00 funded by MCIN/AEI/10.13039/501100011033/FEDER, UE) is gratefully acknowledged. Moreover, this work was funded by the Xunta de Galicia (GRC ED431C 2024/06). M. O. L. thanks the Xunta de Galicia for his "Axudas de apoio á etapa predoutoral" grant (ED481A 2022/236). This work was done within the framework of project HI_MOV – "Corredor Tecnológico Transfronterizo de Movilidad con Hidrógeno Renovable", with reference 0160_HI_MOV_1_E, co-financed by the European Regional Development fund (ERDF), in the scope of Interreg VI A Spain – Portugal Cooperation Program (POCTEP) 2021-2027. This work is part of the project CNS2023-144785, funded by MCIN/AEI /10.13039/501100011033 and the European Union "NextGenerationEU"/PRTR. H. M. C. thanks the USC for his "Convocatoria de Recualificación do Sistema Universitario Español-Margarita Salas" postdoctoral grant under the "Plan de Recuperación Transformación" program funded by the Spanish Ministry of Universities with European Union's NextGenerationEU funds. The authors acknowledge HPC resources granted by GENCI, France (resources of IDRIS, Grant No. 2023-A0140910463).

DATA AVAILABILITY STATEMENT

DFT calculations were carried out using Gaussian 16, revision D.01 (https://gaussian.com/),[66] Psi4 version, 1.9.1 (https://psicode.org/)[67] and Gpaw, version 22.1.0 (https://gpaw.readthedocs.io/).[68] Initial configurations for MD were generated with PACKMOL (https://m3g.github.io/packmol/).[40] MD simulations were performed using OpenMM (https://openmm.org/)[37] and JaxMD (https://github.com/jax-md/jax-md).[69] MD trajectories were postprocessed using MDAnalysis (https://www.mdanalysis.org/),[70,71] Matplotlib (https://matplotlib.org/),[72] Numpy (https://numpy.org/),[73] kute (https://gitlab.com/nafomat/kute),[61] Gnuplot (http://www.gnuplot.info/) and TRAVIS (http://www.travis-analyzer.de/).[74,75]
The data that support the findings of this study are available from the corresponding authors upon request.

V. REFERENCES

[1] M. Armand and J.-M. Tarascon, "Building better batteries," Nature **451**, 652–657 (2008).
[2] P. Simon and Y. Gogotsi, "Perspectives for electrochemical capacitors and related devices," Nat. Mater. **19**, 1151–1163 (2020).
[3] G. Walden, J. Stepan, and C. Mikolajczak, "Safety considerations when designing portable electronics with electric double-layer capacitors (supercapacitors)," in *2011 IEEE Symposium on Product Compliance Engineering Proceedings* (IEEE, 2011) pp. 1–5.
[4] Q. Wang, L. Jiang, Y. Yu, and J. Sun, "Progress of enhancing the safety of lithium ion battery from the electrolyte aspect," Nano Energy **55**, 93–114 (2019).
[5] A. Lewandowski and A. Świderska-Mocek, "Ionic liquids as electrolytes for li-ion batteries—an overview of electrochemical studies," J. Power sources **194**, 601–609 (2009).
[6] M. Salanne, "Ionic Liquids for Supercapacitor Applications," Top. Curr. Chem. **375**, 63 (2017).
[7] W. Zhou, M. Zhang, X. Kong, W. Huang, and Q. Zhang, "Recent advance in ionic-liquid-based electrolytes for rechargeable metal-ion batteries," Adv. Sci. **8**, 2004490 (2021).
[8] M. Galiński, A. Lewandowski, and I. Stępniak, "Ionic liquids as electrolytes," Electrochim. acta **51**, 5567–5580 (2006).
[9] D. S. Silvester and R. G. Compton, "Electrochemistry in room temperature ionic liquids: a review and some possible applications," Z. Phys. Chem. **220**, 1247–1274 (2006).
[10] H. Liu, Y. Liu, and J. Li, "Ionic liquids in surface electrochemistry," Phys. Chem. Chem. Phys. **12**, 1685–1697 (2010).
[11] K. Ghandi, "A review of ionic liquids, their limits and applications," Green Sustain. Chem. **2014** (2014).
[12] E. Jónsson, "Ionic liquids as electrolytes for energy storage applications–a modelling perspective," Energy Storage Mater. **25**, 827–835 (2020).
[13] Z. Lin, E. Goikolea, A. Balducci, K. Naoi, P.-L. Taberna, M. Salanne, G. Yushin, and P. Simon, "Materials for supercapacitors: When li-ion battery power is not enough," Mater. Today **21**, 419–436 (2018).
[14] C. Zhao, G. Burrell, A. A. Torriero, F. Separovic, N. F. Dunlop, D. R. MacFarlane, and A. M. Bond, "Electrochemistry of room temperature protic ionic liquids," J. Phys. Chem. B. **112**, 6923–6936 (2008).
[15] S. Menne, J. Pires, M. Anouti, and A. Balducci, "Protic ionic liquids as electrolytes for lithium-ion batteries," Electrochem. commun. **31**, 39–41 (2013).
[16] S. Ketabi, B. Decker, and K. Lian, "Proton conducting ionic liquid electrolytes for liquid and solid-state electrochemical pseudocapacitors," Solid State Ion. **298**, 73–79 (2016).
[17] A. Djire, J. Y. Ishimwe, S. Choi, and L. T. Thompson, "Enhanced performance for early transition metal nitrides via pseudocapacitance in protic ionic liquid electrolytes," Electrochem. commun. **77**, 19–23 (2017).
[18] J. S. Seenath, D. Pech, and D. Rochefort, "Investigation of protic ionic liquid electrolytes for porous ruo2 micro-supercapacitors," J. Power Sources **548**, 232040 (2022).
[19] M. Anouti, E. Couadou, L. Timperman, and H. Galiano, "Protic ionic liquid as electrolyte for high-densities electrochemical double layer capacitors with activated carbon electrode material," Electrochim. Acta **64**, 110–117 (2012).
[20] R. Mysyk, E. Raymundo-Piñero, M. Anouti, D. Lemordant, and F. Béguin, "Pseudo-capacitance of nanoporous carbons in pyrrolidinium-based protic ionic liquids," Electrochem. commun. **12**, 414–417 (2010).
[21] P. Martínez-Crespo, M. Otero-Lema, O. Cabeza, H. Montes-Campos, and L. M. Varela, "Structure, dynamics and ionic conductivities of ternary ionic liquid/lithium salt/dmso mixtures," J. Mol. Liq. **359**, 119188 (2022).
[22] M. Otero-Lema, P. Martínez-Crespo, T. Méndez-Morales, H. Montes-Campos, and L. M. Varela, "Interfacial structure of protic and aprotic ionic liquid-dmso-li salt mixtures near charged

and neutral electrodes: A molecular dynamics study," J. Mol. Liq. **386**, 122492 (2023).
[23]R. Lois-Cuns, M. Otero-Lema, A. Rivera-Pousa, P. Vallet, J. J. Parajó, O. Cabeza, H. Montes-Campos, T. Méndez-Morales, and L. M. Varela, "Mixtures of ethylammonium nitrate and ethylene carbonate: Bulk and interfacial analysis," J. Mol. Liq. **385**, 122361 (2023).
[24]K. Xu, "Electrolytes and interphases in li-ion batteries and beyond," Chem. Rev. **114**, 11503–11618 (2014).
[25]B. Yang, A. Hu, T. Li, K. Li, Y. Li, J. Jiang, Z. Xiao, Z. W. Seh, and J. Long, "Eliminating water hazards and regulating electrode-electrolyte interfaces by multifunctional sacrificial electrolyte additives for long-life lithium metal batteries," Energy Storage Mater. , 103512 (2024).
[26]T. Stettner, S. Gehrke, P. Ray, B. Kirchner, and A. Balducci, "Water in protic ionic liquids: properties and use of a new class of electrolytes for energy-storage devices," ChemSusChem **12**, 3827–3836 (2019).
[27]L. Dick, T. Stettner, Y. Liu, S. Liu, B. Kirchner, and A. Balducci, "Hygroscopic protic ionic liquids as electrolytes for electric double layer capacitors," Energy Storage Mater. **53**, 744–753 (2022).
[28]K. Goloviznina, Z. Gong, and A. A. H. Padua, "The cl&pol polarizable force field for the simulation of ionic liquids and eutectic solvents," Wiley Interdiscip. Rev. Comput. Mol. Sci. **12**, e1572 (2022).
[29]F. Joerg and C. Schröder, "Polarizable molecular dynamics simulations on the conductivity of pure 1-methylimidazolium acetate systems," Phys. Chem. Chem. Phys. **24**, 15245–15254 (2022).
[30]F. Joerg, J. Sutter, L. van Dam, K. Kanellopoulos, J. Hunger, and C. Schröder, "Comparative analysis of dielectric spectra in protic ionic liquids: Experimental findings and computational molecular decomposition," J. Mol. Liq. **396**, 123834 (2024).
[31]A. Le Donne and E. Bodo, "Isomerization patterns and proton transfer in ionic liquids constituents as probed by ab-initio computation," J. Mol. Liq. **249**, 1075–1082 (2018).
[32]H. Montes-Campos, J. Carrete, S. Bichelmaier, L. M. Varela, and G. K. Madsen, "A differentiable neural-network force field for ionic liquids," J. Chem. Inf. Model. **62**, 88–101 (2021).
[33]F. Joerg, M. Wieder, and C. Schröder, "Protex—a python utility for proton exchange in molecular dynamics simulations," Front. Chem. **11**, 1140896 (2023).
[34]M. Gödény, F. Joerg, M. P.-P. Kovar, and C. Schröder, "Updates to protex for simulating proton transfers in an ionic liquid," J. Phys. Chem. B **128**, 3416–3426 (2024).
[35]M. L. Hoarfrost, M. Tyagi, R. A. Segalman, and J. A. Reimer, "Proton hopping and long-range transport in the protic ionic liquid [im][tfsi], probed by pulsed-field gradient nmr and quasi-elastic neutron scattering," J. Phys. Chem. B **116**, 8201–8209 (2012).
[36]A. A. Moses and C. Arntsen, "Ab initio molecular dynamics study of proton transport in imidazolium-based ionic liquids with added imidazole," Phys. Chem. Chem. Phys. **25**, 2142–2152 (2023).
[37]P. Eastman, J. Swails, J. D. Chodera, R. T. McGibbon, Y. Zhao, K. A. Beauchamp, L.-P. Wang, A. C. Simmonett, M. P. Harrigan, C. D. Stern, *et al.*, "Openmm 7: Rapid development of high performance algorithms for molecular dynamics," (2017).
[38]K. Goloviznina, J. N. Canongia Lopes, M. Costa Gomes, and A. A. H. Padua, "Transferable, Polarizable Force Field for Ionic Liquids," J. Chem. Theory Comput. **15**, 5858–5871 (2019).
[39]J. N. Canongia Lopes and A. Pádua, "Cl&p: A generic and systematic force field for ionic liquids modeling," Theor. Chem. Acc. **131** (2012).
[40]L. Martínez, R. Andrade, E. G. Birgin, and J. M. Martínez, "PACKMOL: A package for building initial configurations for molecular dynamics simulations," J. Comp. Chem. **30**, 2157–2164 (2009).
[41]A. A. H. Padua, "github.com/paduagroup/fftool," (2024).
[42]A. A. H. Padua, "github.com/paduagroup/pol_openmm," (2024).
[43]U. Essmann, L. Perera, M. L. Berkowitz, T. Darden, H. Lee, and L. G. Pedersen, "A smooth particle mesh ewald method," J. Chem. Phys. **103**, 8577–8593 (1995).
[44]Z. Gong and A. A. Padua, "Effect of side chain modifications in imidazolium ionic liquids on the properties of the electrical double layer at a molybdenum disulfide electrode," (2021).
[45]K.-H. Chow and D. M. Ferguson, "Isothermal-isobaric molecular dynamics simulations with monte carlo volume sampling," Comput. Phys. Commun. **91**, 283–289 (1995).
[46]J. Åqvist, P. Wennerström, M. Nervall, S. Bjelic, and B. O. Brandsdal, "Molecular dynamics simulations of water and biomolecules with a monte carlo constant pressure algorithm," Chem. Phys. Lett. **384**, 288–294 (2004).
[47]R. Jacobi, F. Joerg, O. Steinhauser, and C. Schröder, "Emulating proton transfer reactions in the pseudo-protic ionic liquid 1-methylimidazolium acetate," Phys. Chem. Chem. Phys. **24**, 9277–9285 (2022).
[48]J. Carrete, H. Montes-Campos, R. Wanzenböck, E. Heid, and G. K. Madsen, "Deep ensembles vs committees for uncertainty estimation in neural-network force fields: Comparison and application to active learning," J. Chem. Phys. **158** (2023).
[49]J. Enkovaara, C. Rostgaard, J. J. Mortensen, J. Chen, M. Dułak, L. Ferrighi, J. Gavnholt, C. Glinsvad, V. Haikola, H. Hansen, *et al.*, "Electronic structure calculations with gpaw: a real-space implementation of the projector augmented-wave method," J. Phys. Condens. Matter **22**, 253202 (2010).
[50]V. R. Cooper, "Van der waals density functional: An appropriate exchange functional," Phys. Rev. B - Condens. Matter Mater. Phys. **81**, 161104 (2010).
[51]S. S. Schoenholz and E. D. Cubuk, "Jax md: End-to-end differentiable, hardware accelerated, molecular dynamics in pure python," (2019).
[52]D. J. Evans and B. L. Holian, "The nose–hoover thermostat," J. Chem. Phys. **83**, 4069–4074 (1985).
[53]T. Yasuda and M. Watanabe, "Protic ionic liquids: Fuel cell applications," MRS Bull. **38**, 560–566 (2013).
[54]D. Bedrov, J.-P. Piquemal, O. Borodin, A. D. MacKerell, B. Roux, and C. Schröder, "Molecular Dynamics Simulations of Ionic Liquids and Electrolytes Using Polarizable Force Fields," Chem. Rev. **119**, 7940–7995 (2019).
[55]T. Makino, M. Kanakubo, Y. Masuda, T. Umecky, and A. Suzuki, "Co2 absorption properties, densities, viscosities, and electrical conductivities of ethylimidazolium and 1-ethyl-3-methylimidazolium ionic liquids," Fluid Ph. Equilib. **362**, 300–306 (2014).
[56]M. Hasani, L. M. Varela, and A. Martinelli, "Short-range order and transport properties in mixtures of the protic ionic liquid [c2him][tfsi] with water or imidazole," J. Phys. Chem. B **124**, 1767–1777 (2020).
[57]T. Vogl, P. Goodrich, J. Jacquemin, S. Passerini, and A. Balducci, "The influence of cation structure on the chemical–physical properties of protic ionic liquids," J. Phys. Chem. C **120**, 8525–8533 (2016).
[58]I. Abdurrokhman, K. Elamin, O. Danyliv, M. Hasani, J. Swenson, and A. Martinelli, "Protic ionic liquids based on the alkylimidazolium cation: effect of the alkyl chain length on structure and dynamics," J. Phys. Chem. B **123**, 4044–4054 (2019).
[59]I.-C. Yeh and G. Hummer, "System-size dependence of diffusion coefficients and viscosities from molecular dynamics simulations with periodic boundary conditions," J. Phys. Chem. B. **108**, 15873–15879 (2004).
[60]E. J. Maginn, R. A. Messerly, D. J. Carlson, D. R. Roe, and J. R. Elliot, "Best practices for computing transport properties 1. self-diffusivity and viscosity from equilibrium molecular dynamics [article v1. 0]," J. Comp. Mol. Sci. **1**, 6324–6324 (2019).
[61]M. Otero-Lema, R. Lois-Cuns, M. A. Boado, H. Montes-Campos, T. Méndez-Morales, and L. M. Varela, "gitlab.com/nafomat/kute," (2024).
[62]C. Schröder, M. Haberler, and O. Steinhauser, "On the computation and contribution of conductivity in molecular ionic liquids,"

J. Chem. Phys. **128** (2008).
[63]C. Schröder and O. Steinhauser, "On the dielectric conductivity of molecular ionic liquids," J. Chem. Phys. **131** (2009).
[64]H. K. Kashyap, H. V. Annapureddy, F. O. Raineri, and C. J. Margulis, "How is charge transport different in ionic liquids and electrolyte solutions?" J. Phys. Chem. B **115**, 13212–13221 (2011).
[65]K. T. Munson, J. Vergara, L. Yu, and T. D. Vaden, "Characterization of the bridged proton structure in htfsi acid ionic liquid solutions," J. Phys. Chem. B. **119**, 6304–6310 (2015).
[66]M. J. Frisch, G. W. Trucks, H. B. Schlegel, G. E. Scuseria, M. A. Robb, J. R. Cheeseman, G. Scalmani, V. Barone, G. A. Petersson, H. Nakatsuji, X. Li, M. Caricato, A. V. Marenich, J. Bloino, B. G. Janesko, R. Gomperts, B. Mennucci, H. P. Hratchian, J. V. Ortiz, A. F. Izmaylov, J. L. Sonnenberg, D. Williams-Young, F. Ding, F. Lipparini, F. Egidi, J. Goings, B. Peng, A. Petrone, T. Henderson, D. Ranasinghe, V. G. Zakrzewski, J. Gao, N. Rega, G. Zheng, W. Liang, M. Hada, M. Ehara, K. Toyota, R. Fukuda, J. Hasegawa, M. Ishida, T. Nakajima, Y. Honda, O. Kitao, H. Nakai, T. Vreven, K. Throssell, J. A. Montgomery, Jr., J. E. Peralta, F. Ogliaro, M. J. Bearpark, J. J. Heyd, E. N. Brothers, K. N. Kudin, V. N. Staroverov, T. A. Keith, R. Kobayashi, J. Normand, K. Raghavachari, A. P. Rendell, J. C. Burant, S. S. Iyengar, J. Tomasi, M. Cossi, J. M. Millam, M. Klene, C. Adamo, R. Cammi, J. W. Ochterski, R. L. Martin, K. Morokuma, O. Farkas, J. B. Foresman, and D. J. Fox, "Gaussian˜16 Revision B.01," (2016), gaussian Inc. Wallingford CT.
[67]D. G. Smith, L. A. Burns, A. C. Simmonett, R. M. Parrish, M. C. Schieber, R. Galvelis, P. Kraus, H. Kruse, R. Di Remigio, A. Alenaizan, *et al.*, "Psi4 1.4: Open-source software for high-throughput quantum chemistry," (2020).
[68]J. J. Mortensen, A. H. Larsen, M. Kuisma, A. V. Ivanov, A. Taghizadeh, A. Peterson, A. Haldar, A. O. Dohn, C. Schäfer, E. Ö. Jónsson, *et al.*, "Gpaw: An open python package for electronic structure calculations," J. Chem. Phys. **160** (2024).
[69]S. S. Schoenholz and E. D. Cubuk, "Jax m.d. a framework for differentiable physics," in *Advances in Neural Information Processing Systems*, Vol. 33 (Curran Associates, Inc., 2020).
[70]N. Michaud-Agrawal, E. J. Denning, T. B. Woolf, and O. Beckstein, "Mdanalysis: a toolkit for the analysis of molecular dynamics simulations," J. Comput. Chem. **32**, 2319–2327 (2011).
[71]R. J. Gowers, M. Linke, J. Barnoud, T. J. E. Reddy, M. N. Melo, S. L. Seyler, J. Domanski, D. L. Dotson, S. Buchoux, I. M. Kenney, *et al.*, "Mdanalysis: a python package for the rapid analysis of molecular dynamics simulations," Tech. Rep. (Los Alamos National Laboratory (LANL), Los Alamos, NM (United States), 2019).
[72]J. D. Hunter, "Matplotlib: A 2d graphics environment," Comput. Sci. Eng. **9**, 90–95 (2007).
[73]C. R. Harris, K. J. Millman, S. J. Van Der Walt, R. Gommers, P. Virtanen, D. Cournapeau, E. Wieser, J. Taylor, S. Berg, N. J. Smith, *et al.*, "Array programming with numpy," Nature **585**, 357–362 (2020).
[74]M. Brehm and B. Kirchner, "Travis-a free analyzer and visualizer for monte carlo and molecular dynamics trajectories," (2011).
[75]M. Brehm, M. Thomas, S. Gehrke, and B. Kirchner, "Travis—a free analyzer for trajectories from molecular simulation," J. Chem. Phys. **152** (2020).